Journal of Power Sources 195 (2010) 6468–6472

Contents lists available at ScienceDirect

Journal of Power Sources

journal homepage: www.elsevier.com/locate/jpowsour

Short communication

Fabrication and evaluation of the electrochemical performance of the anode-supported solid oxide fuel cell with the composite cathode of $La_{0.8}Sr_{0.2}MnO_{3-\delta}$–Gadolinia-doped ceria oxide/$La_{0.8}Sr_{0.2}MnO_{3-\delta}$

Wei-Xin Kao, Maw-Chwain Lee*, Yang-Chuang Chang, Tai-Nan Lin, Chun-Hsiu Wang, Jen-Chen Chang

Chemical Engineering Division, Institute of Nuclear Energy Research, No. 1000, Wunhua Rd., Jiaan Village, Longtan Township, Taoyuan County 32546, Taiwan, ROC

ARTICLE INFO

Article history:
Received 10 March 2010
Received in revised form 16 April 2010
Accepted 16 April 2010
Available online 24 April 2010

Keywords:
Solid oxide fuel cell
Cathode function layer
Impedance analysis
Contact pressure

ABSTRACT

The anode-supported single cell was constructed with porous Ni–Yittria-stabilized zirconia (YSZ) as the anode substrate, an airtight YSZ as the electrolyte, and a screen-printed $La_{0.8}Sr_{0.2}MnO_{3-\delta}$ (LSM)–Gadolinia-doped ceria (GDC)/LSM double-layer cathode. The SEM results show that the YSZ thin film is highly integrated, fully dense with a thickness of 13 μm, and exhibits excellent compatibility between cathode and electrolyte layers. The effects of feed rates of the reactants, temperature, and contact pressure between the current collector and the unit cell were systematically investigated. The results are based on the assumption that the anode contribution to the polarization resistance is negligible. Our analysis showed that the electrochemical reaction is limited by mass transfer control when the airflow rate is decreased to 500 ml min^{-1}. The maximum power density is 204.6 mW cm^{-2} at 800 °C with H_2 and air at flow rates of 800 and 2000 ml min^{-1}, respectively. According to the AC-impedance data, the resistances of charge transfer at the electrode/electrolyte interface are 3.79 and 1.90 Ω cm^2. The resistances of oxygen-reduction processes are 3.63 and 1.01 Ω cm^2 at 700 and 800 °C, respectively. The results from the sensitivity analysis of the variation of contact pressure between current collectors and membrane electrode assembly (MEA) show that the influence is enhanced at the regions of the high current density.

1. Introduction

Solid oxide fuel cells (SOFCs) have several advantages, such as high efficiency energy conversion, low-polluting emissions, and high orientation of fuels. Yittria-stabilized zirconia (YSZ) is mainly used as the electrolyte for SOFC because of its high oxygen ionic conductivity and its good mechanical properties. However, high operating temperatures of over 800 °C are required for conventional SOFCs to maintain high oxygen ionic conductivity. In an anode-supported SOFC, cathode polarization resistance is the main cause of cell resistance at intermediate operating temperatures. Therefore, it is essential to improve the cathode layer of the cell by introducing high catalytic activities or high oxygen ionic conductivity to enhance the generation rate of oxygen ions and decrease the operating temperature to develop intermediate-temperature SOFCs (IT-SOFCs). Some fundamental characteristics of suitable cathode material with enhanced electrochemical performance include the following: (1) a high rate of oxygen diffusion through the material to assure rapid diffusion of oxygen; (2) high electronic conductivity; (3) high oxygen ion conductivity; and (4) high catalytic activity for the reduction of oxygen [1–3].

Strontium-doped lanthanum manganite (LSM) has been used extensively as a cathode for YSZ-based SOFC [4–8] because of its thermal expansion, chemical stability, high electronic conductivity and good compatibility with YSZ [5,9]. However, low oxygen ion conductivity and high activation energy of LSMs cause decreased cell performance at reduced operating temperature and cause electrochemical reactions that restrict the triple phase boundary (TPB) at the interface between the electrolyte and electrode. It is known that cathode polarization resistance is the main cause of resistance in the cell at intermediate operating temperatures in anode-supported SOFC [5]. High cathode polarization loss limits the promotion of the performance at reduced temperature.

The electrocatalytic activity of LSM can be improved by adding an oxygen ionic conductor, such as YSZ or Gadolinia-doped ceria (GDC). GDC material has a higher oxygen ionic conductivity than YSZ, especially at temperatures below 800 °C [8]. LSM–GDC composite is known to have better performance than typical LSM cathode material [10]. Therefore, GDC–LSM is coated with YSZ electrolyte, which enhances the cathode electrochemical performance and decreases the cathode polarization resistance. It can be seen

* Corresponding author. Tel.: +886 3 4711400x5930; fax: +886 3 4711411.
E-mail address: mclee@iner.gov.tw (M.-C. Lee).

0378-7753/$ – see front matter © 2010 Elsevier B.V. All rights reserved.
doi:10.1016/j.jpowsour.2010.04.057

as the extending of TPB region from the interface between the electrolyte and cathode into the bulk cathode. Hence, diffusion of oxygen ions from the electrode surface to the electrode/electrolyte interface can be improved.

In this study, an anode-supported SOFC with a screen-printed double-layer cathode (Ni–YSZ (anode)/YSZ (electrolyte)/GDC–LSM (function layer)/LSM (cathode)) was fabricated, and the LSM–GDC/LSM composite cathode was compatible with YSZ electrolyte. The effects of the operation variables of the unit cell performances, such as operation temperature, feed rates of gas reactants, and contact pressure between the current collectors and MEA on the polarization behavior of the cell, have been investigated. The microstructure, electrochemical performance, and AC-impedance analysis of the single cell were also examined in this study.

2. Experimental

2.1. Fabrication of the single cell

An anode-supported solid oxide fuel cell with Ni–YSZ (anode)/YSZ (electrolyte)/LSM–GDC (function layer)/LSM (cathode) was fabricated with an active area of about 81 cm^2. The anode substrate was prepared via the tape casting process and sintered at 1400 °C for 4 h. The casting was performed using a tape casting system (ECS, Model CS-8). The YSZ electrolyte was absorbed onto the anode substrate using the spin coating method and sintered at 1400 °C for 4 h. GDC–LSM ink (Fuelcellmaterials com., FCM) was printed onto the YSZ electrolyte layer as a cathode function layer (CFL), and LSM ink (Fuelcellmaterials com., FCM) was printed onto the CFL as a cathode current collector layer (CCCL) using a screen printer and then sintered at 1150 °C for 3 h.

2.2. Characterizations of materials and cell

The morphology of the cross-sections of the single cell was examined using field emission scanning electron microscopy (FE-SEM, Hitachi, S-4800). The composition of the single cell was analyzed using an energy dispersive X-ray spectrometer (EDX, Horiba, 7539H), which is attached to FE-SEM. The cell was set in an in-house-constructed measurement station used for electrochemical property investigation. The cell performance was measured at different operating temperatures with the inlet fuel/oxidant of pure H_2/air. The flow rate of H_2 was fixed at 800 ml min^{-1}. AC-impedance measurements were performed using an impedance analyzer (Solartron 1260) under open circuit conditions with a frequency of 10 kHz to 0.01 Hz.

3. Results and discussion

3.1. Microstructure of the MEA

SEM micrographs of the cross-section of the Ni–YSZ/YSZ/LSM–GDC/LSM cell structure are shown in Fig. 1. It is clear that the YSZ electrolyte layer is fully dense, does not have any cracks, has a thickness of about 13 μm, and exhibits exceptional interfacial contact with the Ni–YSZ electrode and LSM–GDC function layer. It is feasible to prepare a thin electrolyte layer by spin coating onto the anode substrate. The LSM cathode and LSM–GDC functional layers have porous microstructures to assure diffusion of gas. Fig. 2 shows the SEM image of the LSM–GDC/LSM double cathode layers and its elemental distribution, which was obtained by linear scanning analysis using EDX. The thickness of the LSM–GDC functional layer is about 23 μm, which was estimated from the La and Ce signals. The total thickness of the

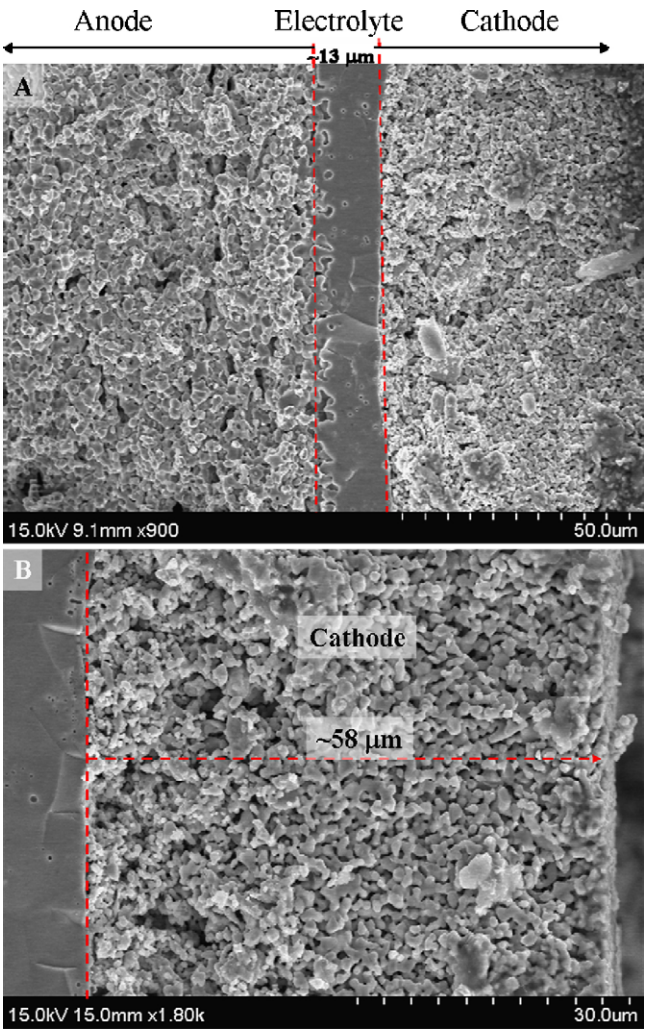

Fig. 1. SEM micrographs of the cross-section of (a) whole cell; and (b) part of the double-layers of the cathode.

cathode layer is about 58 μm, which consists of a 23 μm LSM–GDC layer and a 35 μm LSM layer.

3.2. Cell performance and analysis of electrochemical impedance spectrum

Fig. 3 shows the effect of airflow rate on the impedance of the cell at 800 °C. The cell impedance spectra consist of two semicircles, and this fact indicates that at least two different electrode processes occurred corresponding to the high- and low-frequency arcs during the electrochemical reduction of the cell. According to prior reports [11,12], the high-frequency arc can be attributed to the migration of oxygen ions from the electrode to the electrolyte, and the low-frequency arc can be attributed to the oxygen-reduction processes. Several steps are involved in the mechanism of the oxygen-reduction process, including oxygen transfer, dissociative adsorption, and surface diffusion of oxygen intermediate species on the electrode. Because the contribution of anode polarization is relatively small, the electrode resistance of the cell is mainly attributed to cathode polarization [11,13]. In high-frequency range, the impedance spectra were almost invariant with the different airflow rates. However, the impedance obviously increased when the airflow rate was decreased to 500 ml min^{-1} in low-frequency range. This suggests that the increased impedance is due to limitations of gas diffusion in the cathode layer [14], and that a high

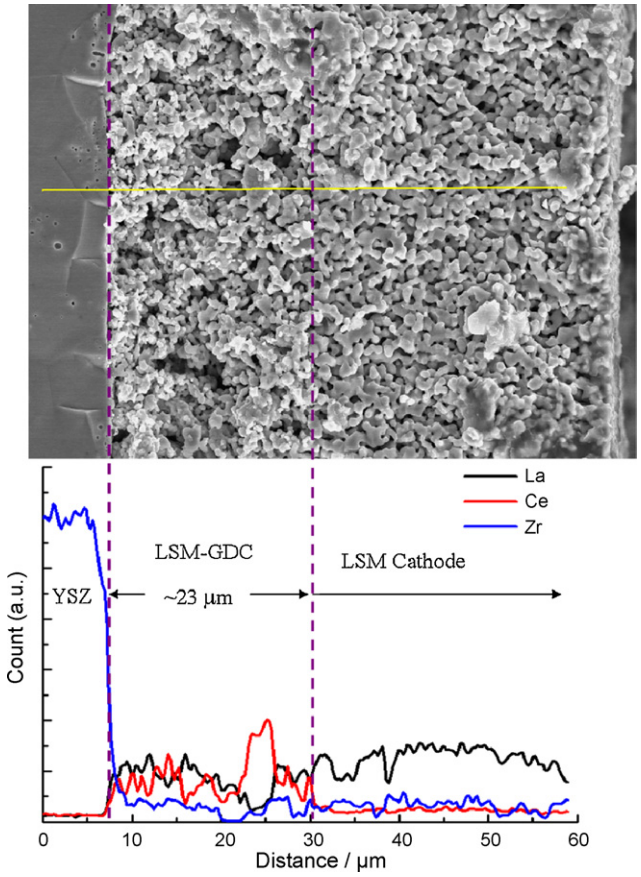

Fig. 2. EDX analyses of the LSM–GDC/LSM double cathode layers with linear scanning analysis of elements.

airflow rate improves mass transfer in the cathode without influencing the electrochemical kinetics of the cell. This also shows that the electrochemical limitation is transferred progressively to the oxygen transport with a decrease in the airflow rate because the decreasing airflow rate would increase the thickness of the diffusion layer near the cathode reaction surface and influence the cell performance [8].

The cell performance tests were executed with an operating temperature range of 700–800 °C. The results of the *I–V* and *I–P* curves are presented in Fig. 4. The maximum power densities are 80.7, 137.8, and 204.6 mW cm^{-2} at temperatures of 700, 750, and

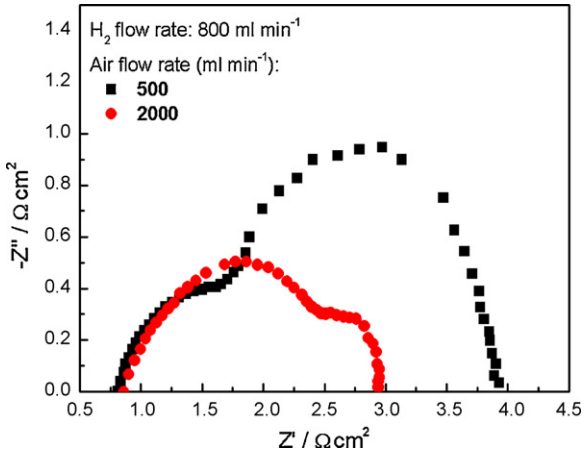

Fig. 3. The effect of air flow rate on the impedance measured at 800 °C.

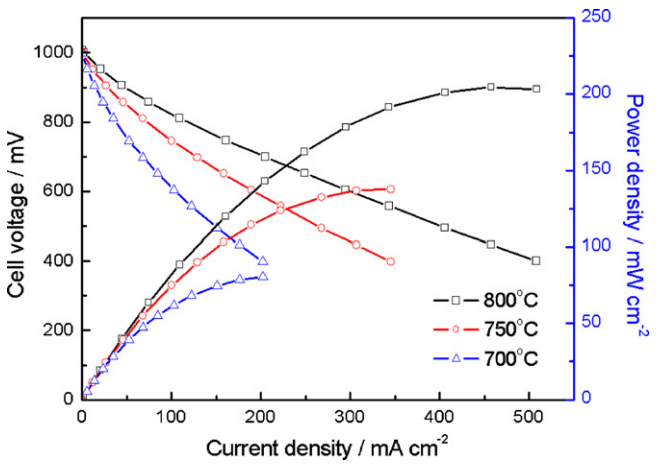

Fig. 4. Cell performance measured at different operating temperatures.

800 °C, respectively. The H_2 fuel and air oxidant flow rates were 800 and 2000 ml min^{-1}. The performance of the single cell was increased by increasing the operating temperature. For cell testing, the measured OCV values were in the range of 1.0–1.1 V at 800 °C. After the initial activation operation, the OCV was constantly higher than 1.0 V (max. 1.05 V). This indicates that no gas leakage occurred through the YSZ electrolyte layer of the cell, and no cracks were present on the YSZ film. This result is in agreement with the investigation of SEM observation.

Fig. 5(a) shows the impedance spectra of the cell at different operating temperatures. The equivalent circuit is presented in Fig. 5(b), and the fitting results using Zview software are listed in Table 1. In the equivalent circuit, R_E corresponds to the ohmic resistance from the electrolyte, electrodes and the connection

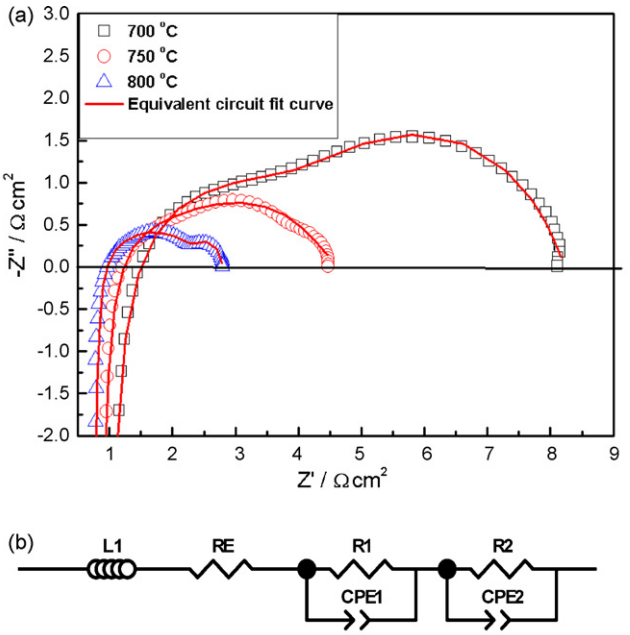

L: Inductor due to Pt wire and electrode wire
R_E: Ohmic resistance
CPE_1:High frequency region constant phase element (CPE)
R_1: The resistance of charge-transfer at electrode/electrolyte interface
CPE_2: Low frequency region constant phase element (CPE)

Fig. 5. (a) Impedance spectra of unit cell at different operating temperatures. (b) Equivalent circuit.

Table 1
Fitting parameters from AC-impedance results obtained at different temperatures.

	Temperature (°C)		
	700	750	800
R_E (Ω cm^2)	0.80	0.70	0.66
R_1 (Ω cm^2)	3.79	2.10	1.9
R_2 (Ω cm^2)	3.63	1.77	1.01
R_p (Ω cm^2)	7.42	3.87	2.91

wire resistances. L corresponds to inductance, which is attributed to the Pt current–voltage probes or the high-frequency phase shift of the electrochemical equipment [11,12]. The resistance R_1 results from oxygen ion transfer from TPB to YSZ electrolyte film [11]. The resistance R_2 is related to the resistance from oxygen-reduction processes in the cathode. CPE_1 and CPE_2 represent the constant phase elements of high- and low-frequency arcs [11]. At 700, 750, and 800 °C, the resistances (R_1) are 3.79, 2.10, and 1.90 Ω cm^2, respectively, and the resistances (R_2) are 3.63, 1.77, and 1.01 Ω cm^2, respectively. All types of resistance decreased with increasing temperature, which indicates that oxygen ion transfer at the electrode–electrolyte interface and YSZ electrolyte film, as well as oxygen-reduction, were enhanced by increasing the temperature. At 700 °C, the high-frequency resistance (R_1) and low-frequency resistance (R_2) are very close, which indicates that the electrochemical reaction on the cathode is governed by oxygen ion migration from the cathode to the YSZ electrolyte and oxygen-reduction processes in the cathode. The values of R_1 divided by R_2 are progressively enhanced from 1.04 to 1.88 with increasing temperature, which indicates that the limitation of the electrochemical reaction on the cathode has become the transfer of oxygen ions at the interface between the cathode and electrolyte at higher operation temperature. The reduction of the polarization resistance (R_1 and R_2) is mainly governed by the resistance (R_1) at the temperature above 800 °C.

The total resistance ($R_E + R_P$) of the unit cell is mainly governed by the polarization resistance, which decreases from 90.2% at 700 °C to 81.5% at 800 °C. This indicates that the polarization of the cell needs to be reduced to improve the cell performance. According to the information of Table 1 and Fig. 4, the performance of the cell is significantly limited by electrode polarization (R_p), which dominates cell resistance, and the effect of electrode polarization on the total cell resistance ($R_E + R_P$) decreases with increasing operating temperature.

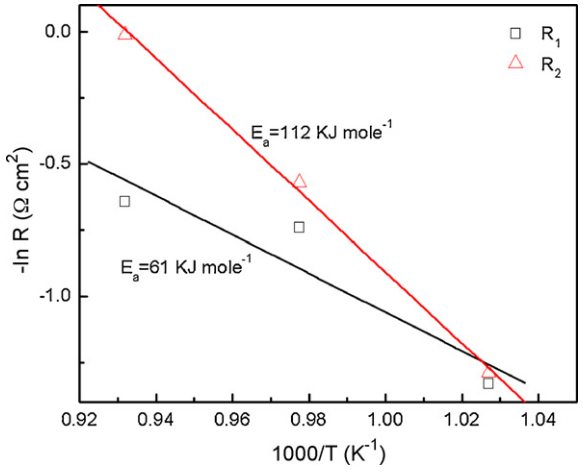

Fig. 6. Arrhenius plots of the polarization resistances (R_1 and R_2) measured at difference temperatures.

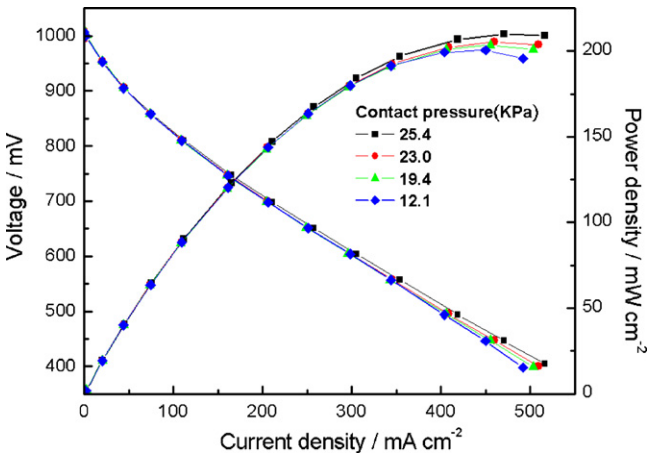

Fig. 7. Effect of contact pressure between current collector and MEA on cell performance measured at 800 °C.

Fig. 6 shows the Arrhenius plot of polarization resistance for the cathode. The values used for the fitting might be scattered, which results in considerable uncertainty in the activation energy value. Based on the Arrhenius plot, the activation energies (E_a) of polarization resistance due to oxygen ion transfer at electrode/electrolyte interface (R_1) and oxygen-reduction processes (R_2) are estimated to be 61 and 112 kJ mol^{-1}, respectively. The activation energy of R_1 (61 kJ mol^{-1}) is lower than the activation energy of oxygen ions migration from TPB into YSZ electrolyte (107 kJ mol^{-1}) [11]. In contrast, the activation energy of oxygen-reduction processes on the LSM cathode is 156.3 kJ mol^{-1} [11], which is higher than that of the LSM–GDC/LSM cathode (R_2, 112 kJ mol^{-1}). As discussed above, these results can be attributed to the addition of high ionic conductivity material (GDC) in the LSM cathode that functions to accelerate oxygen-reduction processes and to enhance oxygen ion transport from reaction sites to TPB.

3.3. *The influences of the contact pressure between current collector and MEA on cell performance*

Cell performance tests were executed by applying different weight loads to the MEA-current collector at 800 °C. The results are shown in Fig. 7. The contact pressure is calculated as the ratio of weight load over cathode area. From the I–V curves, the apparent cell resistance decreases, and the maximum power density increases from 200.6 to 214.1 mW cm^{-2} by increasing contact pressure from 12.1 to 25.4 kPa. At low-current density (reaction region), the variation of V–I plots is not prominent under various weight loads. At high current density (ohmic polarization region), the effects of the weight load on cell performance are obvious. This indicates that increasing contact pressure improves ohmic resistance of the cell and has no influence on the electrode kinetics. This result is in agreement with the report by Holtappels and Bagger [15]. Hence, the decreased resistance can be attributed to the ohmic part of the cell. Ohmic resistance is determined by the electrolyte structure, the current collector, and the circuit of the measurement system. The ohmic resistance of the circuit of the measurement system and the electrolyte structure are assumed to have no impact under various weight loads. The decreasing ohmic resistance is mainly attributed to the current pickup part of the cell. According to the above discussion, the electrical conductivity should be affected by the contact pressure applied to the current collector on the cell. This means that the electrical conductivity between the cell and the measurement system significantly influences the overall performance of the cell. Hence, the resistances from the AC-impedance test are in good agreement with the results of the performance test.

4. Conclusions

The effects of operation conditions on performance of an anode-supported SOFC (Ni–YSZ/YSZ/LSM–GDC/LSM) were investigated. Evaluation of the results was based on the assumption that the contribution of the anode to polarization resistance was negligible. For the performance test of the anode-supported cell, the maximum power densities obtained were 80.7, 137.8, and 204.6 mW cm^{-2} at 700, 750, and 800 °C, respectively. The performance of the cell increased with elevated temperature due to the decrease in resistance of the whole cell with increasing operating temperature. Therefore, the values from the performance test are in good agreement with the results from the AC-impedance analysis. The AC-impedance analysis showed that the total resistance of the cell is primarily governed by oxygen-reduction processes on the LSM–GDC/LSM cathode in the temperature range of 700–800 °C. A high airflow rate improves mass transfer in the cathode without influencing the electrochemical kinetics of the cell.

The LSM–GDC/LSM composite cathode improved the activity of oxygen-reduction processes and showed a lower activation energy than the LSM cathode. The ASR of the LSM–GDC/LSM cathode for high-frequency resistances (R_1) of the electrodes were 3.79, 2.10, and 1.90 Ω cm^2, and the low-frequency resistances (R_2) were 3.63, 1.77, and 1.01 Ω cm^2 at 700, 750, and 800 °C, respectively. The activation energies of R_1 and R_2 are estimated to be 61 and 112 kJ mol^{-1}, respectively. The LSM–GDC cathode functions to accelerate the oxygen-reduction processes and enhance oxygen ion transfer from the reaction sites to TPB. However, it is important to develop novel cathode materials or improve the electrode structure to improve the performance of the cell. Increasing the contact pressure improves ohmic resistance of the cell and has no influence on electrode kinetics. The contact pressure should affect the electrical conductivity between the cell and the current collector. The contact pressure between current collectors and MEA must be kept high enough to enhance the overall cell performance.

References

[1] G.C. Corbel, S. Mestiri, P. Lacorre, Solid State Sci. 7 (2005) 1216–1224.
[2] S. Li, Z. Lu, B. Wei, X. Huang, J. Miao, G. Gao, R. Zhu, W. Su, J. Alloys Compd. 426 (2006) 408–414.
[3] A.C. Van, M. Veen, D. Rebeilleau, C. Farrusseng, Mirodatos, Chem. Commun. 9 (2003) 32–33.
[4] V.A.C. Haanappel, J. Mertens, D. Rutenbeck, C. Tropartz, W. Herzhof, D. Sebold, F. Tietz, J. Power Sources 141 (2005) 216–226.
[5] K. Chen, Z. Lü, X. Chen, N. Ai, X. Huang, X. Du, W. Su, J. Power Sources 172 (2005) 742–748.
[6] T. Horita, K. Yamaji, N. Sakai, H. Yokokawa, T. Kawada, T. Kato, Solid State Ionics 127 (2000) 55–65.
[7] A. Hagiwara, N. Hobara, K. Takizawa, K. Sato, H. Abe, M. Naitio, Solid State Ionics 177 (2006) 2967–2977.
[8] P. Leone, M. Santarelli, P. Asinari, M. Calì, R. Borchiellini, J. Power Sources 177 (2008) 111–122.
[9] G. Corbel, S. Mestiri, P. Lacorre, Solid State Sci. 7 (2005) 1216–1224.
[10] S.P. Jiang, W. Wang, Solid State Ionics 176 (2005) 1351–1357.
[11] K.A. Khor, S.H. Chan, J. Power Sources 123 (2003) 17–25.
[12] Y.J. Leng, S.H. Chan, K.A. Khor, S.P. Jiang, Int. J. Hydrogen Energy 29 (2004) 1025–1033.
[13] W.X. Kao, M.C. Lee, T.N. Lin, C.H. Wang, Y.C. Chang, J. Power Sources 195 (2010) 2220–2223.
[14] Q.L. Liu, K.A. Khor, S.H. Chan, X.J. Chen, J. Power Sources 162 (2006) 1036–1042.
[15] P. Holtappels, C. Bagger, J. Eur. Ceram. Soc. 22 (2002) 41–48.